JPE 16-5-2

http://dx.doi.org/10.6113/JPE.2016.16.5.1639
ISSN(Print): 1598-2092 / ISSN(Online): 2093-4718

A Family of Magnetic Coupling DC–DC Converters With Zero-Voltage-Switching Over Wide Input Voltage Range and Load Variation

Guipeng Chen*, Jie Dong*, Yan Deng†, Yong Tao*, Xiangning He*, and Yousheng Wang*

*,†College of Electrical Engineering, Zhejiang University, Hangzhou, China

Abstract

This paper presents a family of soft-switching DC–DC converters with a simple auxiliary circuit consisting of a coupled winding and a pair of auxiliary switch and diode. The auxiliary circuit is activated in a short interval and thus the circulating conduction losses are small. With the auxiliary circuit, zero-voltage-switching (ZVS) and zero-current-switching are achieved for the main and auxiliary switches respectively, over wide input voltage range and load variation. In addition, the reverse-recovery problem of diodes is significantly alleviated because of the leakage inductor. Furthermore, the coupled inductor simultaneously serves as the main and auxiliary inductors, contributing to reduced magnetic component in comparison with the conventional zero-voltage-transition (ZVT) converters. Experimental results based on a 500 W prototype buck circuit validate the advantages and effectiveness of the proposed magnetic coupling ZVS converter.

Key words: DC–DC converters, Magnetic coupling, Zero-current-switching (ZCS), Zero-voltage-switching (ZVS)

I. Introduction

DC–DC converters have been widely applied in the industrial applications, such as in hybrid electric vehicles and renewable energy systems [1], [2]. To attain high density and efficiency, soft-switching techniques are utilized in high-frequency DC–DC converters. Among these techniques, zero-voltage-switching (ZVS) [3]-[26] including quasi-resonant ZVS, active-clamping ZVS, zero-voltage-transition (ZVT), and magnetic coupling ZVS converters have been intensively studied to eliminate turn-on losses, which is the dominant switching losses in the majority carrier devices, such as MOSFET.

Quasi-resonant converters (QRCs) achieve ZVS operation by employing LC resonance to create a zero-voltage turn-on condition [3]-[5]. Switching losses are effectively reduced, but the main switch suffers from excessively high voltage stress because of resonance. Moreover, the switching frequency varies widely under large load variations, thus making the design of passive components difficult. Pulse-width modulation (PWM) can be achieved in active-clamping ZVS converters with the assistance of an auxiliary switch [6]-[10]. However, the circulating current in the auxiliary circuit is large, thus increasing conduction losses. In addition, the voltage stress of the main switch remains high.

Conduction losses are reduced in ZVT converters since the auxiliary circuit is removed from the main circuit and only activated in a short interval around the turn-on of the main switch [11]-[21]. Furthermore, the voltage stress of the main switch is lower than that of QRCs and active-clamping converters. The work in [11] classified ZVT converters into three classes according to the implementation of the auxiliary voltage source (AVS): Class-A with switched AVS [12]-[15], Class-B with DC AVS [16]-[18], and Class-C with resonant AVS [19]-[21]. The characteristics of the main circuit in all these three converters are similar, whereas the performances of their auxiliary circuits are quite different [22]. The auxiliary circuit of Class-A ZVT converters is simple, but their auxiliary switch is zero-current-switching (ZCS) turned on and ZVS turned off, which causes additional switching losses. Improved ZCS turn-on and turn-off is achieved for the auxiliary switch in the Class-B and Class-C ZVT converters.

Manuscript received Dec. 15, 2015; accepted Apr. 20, 2016.
Recommended for publication by Associate Editor Chun-An Cheng.
†Corresponding Author: dengyan@zju.edu.cn
Tel: +86-571-87952416, Fax: +86-571-87951797, Zhejiang University
*College of Electrical Engineering, Zhejiang University, China

But in Class-C ZVT converters with resonant AVS, the design of the resonant tank is complex, and additional reactive energy is introduced. In Class-B ZVT converters, the configuration of the auxiliary circuit remains simple because the DC AVS can be directly obtained from the voltage source of the main circuit. However, the available input voltage range and load variation are limited to ensure that ZVS operation is achieved for the main switch [16], [17].

In references [23]-[26], coupled inductors were employed to achieve ZVS for synchronous DC–DC converters over a wide range of input voltage and load variation. The auxiliary circuit is relatively simple because it is composed of an auxiliary diode and a coupled winding. The magnetic component is reduced since the leakage inductor of the coupled inductor is utilized to function as the auxiliary inductor, which is indispensable in non-isolated QRCs, active-clamping ZVS converters, and ZVT converters. However, the circulating conduction loss in the auxiliary circuit is large because the auxiliary circuit is uncontrolled and activated in a long interval. In [27], circulating conduction losses were reduced with the addition of a switch in series with the auxiliary diode, and the auxiliary circuit was only activated in a short interval. Meanwhile, the controlled auxiliary circuit was also utilized in [28] to achieve ZVS operation for bidirectional DC–DC converters.

The present study proposes a family of magnetic coupling ZVS DC–DC converters. A pair of auxiliary switch and diode is utilized to control the auxiliary circuit, thereby contributing to small circulating conduction losses. Besides, with the assistance of the coupled winding, soft-switching is achieved for both main and auxiliary switches over wide input voltage range and load variation, along with a reduced magnetic component. The paper is organized as follows. Class-B ZVT DC–DC converters are briefly introduced, and a family of magnetic coupling ZVS buck, boost as well as buck-boost converters is derived in Section II. As an example, the operation principle of the proposed ZVS buck converter is shown in Section III. The analysis and comparison results with other ZVS buck converters are provided in Section IV. The experimental results validating the effectiveness of the proposed converter are presented in Section V. Finally, conclusions are drawn in Section VI.

II. TOPOLOGY DERIVATION

In order to gain a clear understanding of the soft-switching principle, Class-B ZVT DC-DC converters which implement DC AVS without additional components, are briefly introduced. ZVS and ZCS can be respectively achieved for main and auxiliary switches with a simple auxiliary circuit. However, ZVS realization is restricted by the input voltage and load condition. To improve the soft-switching characteristic, a family of magnetic coupling DC–DC converters is proposed, which realizes ZVS for the main switch over wide input voltage range as well as load variation. Also, the benefit of ZCS for the auxiliary switch is maintained. Furthermore, no extra auxiliary inductor is needed, contributing to reduced magnetic component.

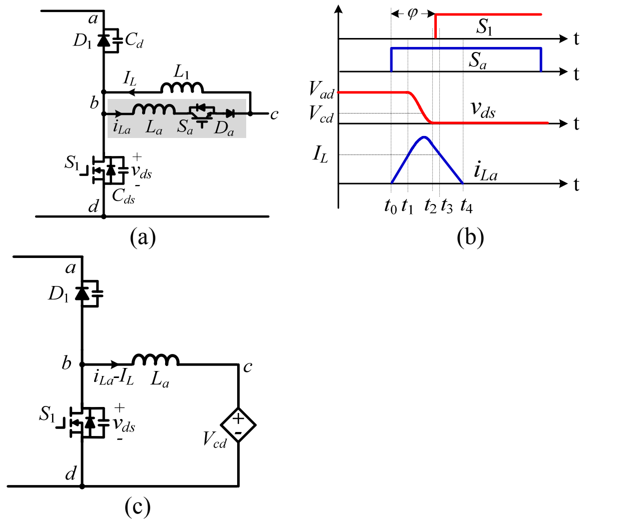

Fig. 1. Class-B ZVT DC-DC converter: (a) general topology, (b) key waveforms, and (c) equivalent circuit in the interval t_0–t_4.

A. Class-B ZVT DC–DC Converters

The general Class-B ZVT DC–DC converter composed of a basic PWM block and a simple auxiliary circuit which implements DC AVS without additional components, is illustrated in Fig. 1(a) [16]-[18]. The basic PWM block consists of the inductor L_1, main diode D_1 with parasitic capacitor C_d, and main switch S_1 with parasitic capacitor C_{ds}. To achieve ZVS for the main switch S_1, the auxiliary circuit makes use of the inductor L_a, switch S_a, and diode D_a to discharge and charge C_{ds} and C_d, respectively. The operation of the converter is the same as that of the conventional DC–DC converter, except when the auxiliary circuit is active. In the active interval, key waveforms including the drive signals of the main and auxiliary switches, drain-to-source voltage v_{ds}, as well as auxiliary inductor current i_{La}, are shown in Fig. 1(b) [11], and the equivalent circuit is illustrated in Fig. 1(c). To simplify the operation principle, the current of inductor L_1 is assumed to be constant and denoted as I_L.

Before t_0, the auxiliary switch S_a is in the off state, and the auxiliary inductor current i_{La} is zero. The switch S_1 is in the off state, and the inductor current I_L flows through the diode D_1.

Stage 1 (t_0–t_1): At t_0, the auxiliary switch S_a is turned on. Then the auxiliary inductor L_a is charged, and i_{La} is linearly increased to I_L at t_1. The interval t_1–t_0 is obtained in (2).

$$i_{La}(t) = \frac{v_{bd} - V_{cd}}{L_a}(t - t_0) = \frac{V_{ad} - V_{cd}}{L_a}(t - t_0) \quad (1)$$

$$t_1 - t_0 = \frac{L_a I_L}{V_{ad} - V_{cd}} \quad (2)$$

Stage 2 (t_1–t_2): In this stage, the equivalent capacitance C_{eq}, which is the sum of parasitic capacitances C_{ds} and C_d, resonates with the auxiliary inductor L_a, as illustrated in (3). Then the voltage v_{ds} and current i_{La} can be derived in (4). At t_2, the voltage v_{ds} decreases to zero, and the resonant process is finished. The interval t_2–t_1 and $i_{La}(t_2)$ are given in (5) and (6), respectively.

$$\begin{cases} C_{eq}\dfrac{dv_{ds}(t)}{dt} = I_L - i_{La}(t), \quad v_{ds}(t_1) = V_{ad} \\ L_a\dfrac{di_{La}(t)}{dt} = v_{ds}(t) - V_{cd}, \quad i_{La}(t_1) = I_L \end{cases} \tag{3}$$

$$\begin{cases} v_{ds}(t) = V_{cd} + (V_{ad} - V_{cd})\cos\omega_1(t-t_1) \\ i_{La}(t) = I_L + \omega_1 C_{eq}(V_{ad} - V_{cd})\sin\omega_1(t-t_1) \end{cases} \tag{4}$$

$$t_2 - t_1 = \frac{1}{\omega_1}\arccos\left(\frac{V_{cd}}{V_{cd} - V_{ad}}\right) \tag{5}$$

$$i_{La}(t_2) = I_L + \sqrt{\frac{C_{eq}}{L_a}(V_{ad}^2 - 2V_{cd}V_{ad})} \tag{6}$$

where $\omega_1 = \dfrac{1}{\sqrt{L_a C_{eq}}}$.

Stage 3 (t_2–t_3): After the complement of the resonant process, the current i_{La}-I_L flows through the anti-parallel diode of switch S_1. Therefore, i_{La} is linearly decreased, and the switch S_1 should be turned on to achieve ZVS operation before i_{La} decays to I_L at t_3. Thus, the phase angle φ between the two drive signals in Fig. 1(b) should satisfy (9).

$$i_{La}(t) = -\frac{V_{cd}}{L_a}(t - t_2) \tag{7}$$

$$t_3 - t_2 = \frac{L_a(I_L - i_{La}(t_2))}{-V_{cd}} = \frac{\sqrt{L_a C_{eq}(V_{ad}^2 - 2V_{cd}V_{ad})}}{V_{cd}} \tag{8}$$

$$(t_2 - t_0) < \varphi / 2\pi \times T_s < (t_3 - t_0) \tag{9}$$

where T_s is the switching period.

Stage 4 (t_3–t_4): The operation in this stage is similar with that of stage 3, except that the current i_{La}-I_L flows from the anti-parallel diode to the MOSFET channel of switch S_1. i_{La} continues to decrease and drops to zero at t_4.

In order to achieve ZVS for the main switch S_1, the parasitic capacitance C_{ds} should be completely discharged in stage 2; thus, the voltage limitation is derived in (10) from (4) [16]. Meanwhile, the limit of maximum inductor current $I_{L,\max}$ is obtained in (11) from (2), (5), (8), and (9) to realize ZVS with a fixed φ over the whole load range. Therefore, the practical applications of Class-B ZVT converters in Fig. 1(a) are restricted.

$$V_{cd} < 0.5V_{ad} \tag{10}$$

$$I_{L,\max} < \frac{V_{ad} - V_{cd}}{V_{cd}}\sqrt{\frac{C_{eq}}{L_a}(V_{ad}^2 - 2V_{cd}V_{ad})} \tag{11}$$

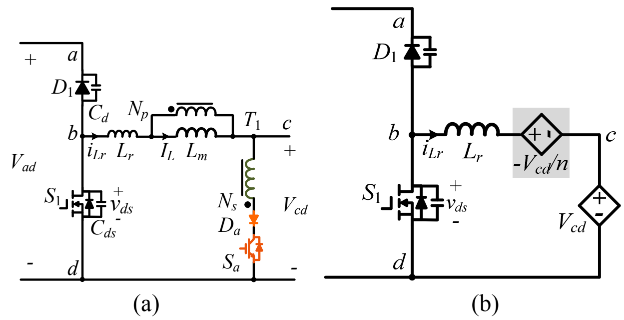

Fig. 2. Proposed general magnetic coupling ZVS DC–DC converter: (a) topology configuration and (b) equivalent circuit in the active interval.

TABLE I
VALUES OF V_{AD} AND V_{CD} FOR PROPOSED ZVS BUCK, BOOST, AND BUCK-BOOST CONVERTERS

	V_{ad}	V_{cd}
buck	V_i	V_i -V_o
boost	V_o	V_i
buck-boost	V_i -V_o	V_i

B. Proposed Magnetic Coupling ZVS DC–DC Converters

In order to achieve ZVS for main switches over wide input voltage range and load variation, a family of magnetic coupling ZVS DC-DC converters is proposed. The general magnetic coupling ZVS DC–DC converter is illustrated in Fig. 2(a). Compared with the Class-B ZVT converter in Fig. 1(a), a coupled inductor T_1 with turns ratio N_p:N_s=1:n is employed to implement the main inductor L_1 with the magnetizing inductor L_m and the auxiliary inductor L_a with the leakage inductor L_r. Thus the magnetic component number is reduced. The secondary winding of the coupled inductor T_1, the auxiliary switch S_a, and the diode D_a are connected in series between ports c and d. The equivalent circuit in the interval when S_a and D_a conduct is shown in Fig. 2(b). Compared with Fig. 1(c), an additional voltage source -V_{cd}/n is added since the secondary voltage of the coupled inductor T_1 is clamped to -V_{cd}. Hence, the limitation in (10) and (11) is modified in (12) and (13), respectively. According to (10), for the Class-B ZVT converter in Fig. 1(a), the ZVS operation of the main switch S_1 can be achieved only when V_{cd} is smaller than 0.5 V_{ad}, which is greatly alleviated in the proposed converter as illustrated in (12). Moreover, the available ZVS load range is also enlarged with the comparison of (13) and (11).

$$(1 - \frac{1}{n})V_{cd} < 0.5V_{ad} \tag{12}$$

$$I_{L,\max} < \frac{V_{ad} - (1-\frac{1}{n})V_{cd}}{(1-\frac{1}{n})V_{cd}}\sqrt{\frac{C_{eq}}{L_r}(V_{ad}^2 - 2(1-\frac{1}{n})V_{cd}V_{ad})} \tag{13}$$

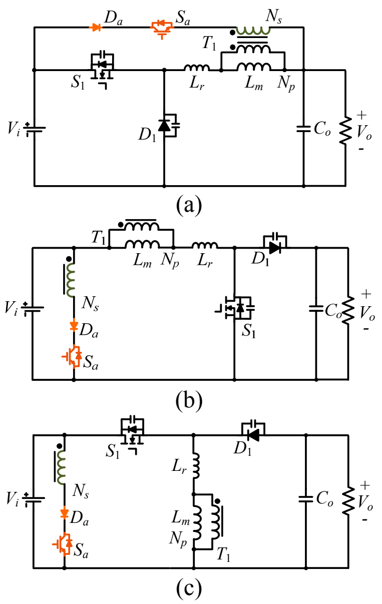

Fig. 3. Proposed magnetic coupling ZVS DC–DC converters: (a) buck, (b) boost, and (c) buck-boost.

On the basis of the general magnetic coupling DC–DC converter in Fig. 2(a), the corresponding ZVS buck, boost, and buck-boost converters with different values for V_{ad} and V_{cd} in the Table I, are derived in Fig. 3. Besides, the magnetic coupling concept can be employed to achieve ZVS operation for various converters which consists of the basic PWM block.

III. Operation Principle

As the operation principles of the proposed magnetic coupling ZVS buck, boost, and buck-boost converters are similar, the ZVS buck converter is used as an example in this section, which is re-shown in Fig. 4(a). Key operating waveforms of the converter are shown in Fig. 4(b). The auxiliary switch S_a is turned on in advance to decrease the leakage inductor current i_{Lr} and create ZVS condition for the main switch S_1. In a switching period, the operation comprises seven stages, and the corresponding equivalent circuits of which are illustrated in Fig. 5.

Several assumptions are made to simplify the operation principle.

—L_m is large; hence, the magnetizing current I_L is assumed to be constant.

—The leakage inductance L_r is much lower than the magnetizing inductance L_m.

—The parasitic capacitances C_{ds} and C_d are constant during the switching process, and their sum is denoted as C_{eq},

—All components are ideal, except for the parasitic capacitances of the main switch and diode.

From Fig. 4(a), the relationship among the leakage inductor current i_{Lr}, auxiliary current i_a, magnetizing current I_L, and output current i_o is derived in (14) and (15).

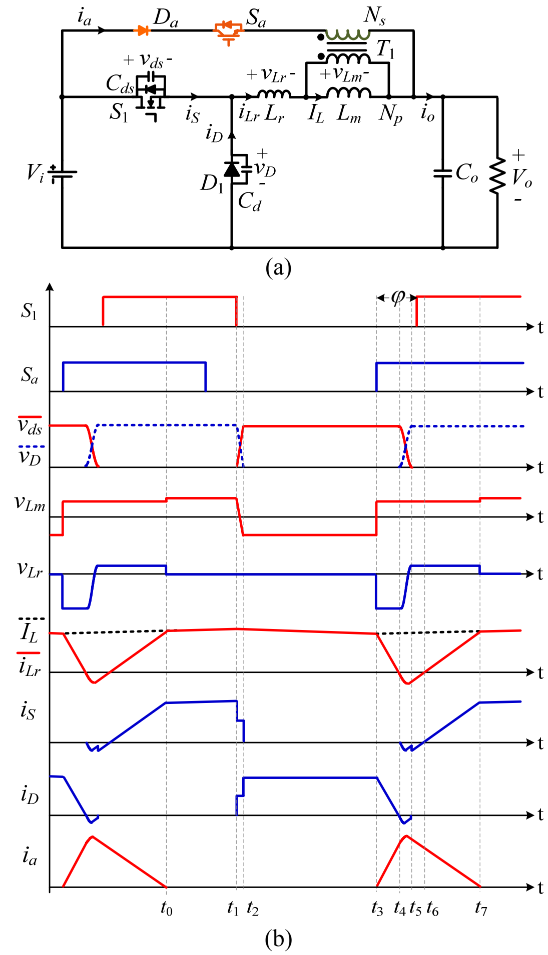

Fig. 4. Proposed magnetic coupling ZVS buck converter: (a) circuit and (b) key waveforms.

$$i_{Lr}(t)+ni_a(t)=I_L \tag{14}$$

$$i_{Lr}(t)+i_a(t)=i_o(t) \tag{15}$$

Prior to t_0, S_1 and S_a are in the on state. The leakage inductor current i_{Lr} is increased, whereas the auxiliary current i_a is decreased.

Stage 1 (t_0–t_1): At t_0, i_{Lr} rises to the magnetizing current I_L, and i_a decays to zero; thus, D_a is reverse biased. In this stage, the energy is transferred from the input to the leakage inductor L_r, magnetizing inductor L_m, and output. Since the auxiliary current i_a is zero, the auxiliary switch S_a is ZCS turned off in this stage.

$$i_S(t)=i_{Lr}(t)=I_L \tag{16}$$

$$v_{Lm}(t)=\frac{L_m}{L_r+L_m}(V_i-V_o) \tag{17}$$

$$v_{Lr}(t)=\frac{L_r}{L_r+L_m}(V_i-V_o) \tag{18}$$

Stage 2 (t_1–t_2): S_1 is turned off at t_1. The parasitic capacitors C_{ds} and C_d are respectively charged and discharged by I_L. Therefore, the drain-to-source voltage v_{ds} increases linearly, as shown in (19).

$$v_{ds}(t)=\frac{I_L}{C_{eq}}(t-t_1) \quad (19)$$

$$v_{Lm}(t)=\frac{L_m}{L_r+L_m}(V_i-V_o-v_{ds}(t)) \quad (20)$$

$$v_{Lr}(t)=\frac{L_r}{L_r+L_m}(V_i-V_o-v_{ds}(t)) \quad (21)$$

Stage 3 (t_2–t_3): At t_2, v_{ds} increases to V_i; hence, the main switch D_1 is forward biased. During this stage, the energy is transferred from the leakage inductor L_r and magnetizing inductor L_m to the output.

$$i_D(t)=i_{Lr}(t)=I_L \quad (22)$$

$$v_{Lm}(t)=-\frac{L_m}{L_r+L_m}V_o \quad (23)$$

$$v_{Lr}(t)=-\frac{L_r}{L_r+L_m}V_o \quad (24)$$

Stage 4 (t_3–t_4): At t_3, the auxiliary switch S_a is turned on, and the magnetizing voltage v_{Lm} is clamped to $(V_i-V_o)/n$. In this stage, the leakage inductor current i_{Lr} and the diode current i_D decrease linearly, as shown in (27). Based on (14), the auxiliary current i_a increases.

$$v_{Lm}(t)=\frac{V_i-V_o}{n} \quad (25)$$

$$v_{Lr}(t)=-\frac{V_i+(n-1)V_o}{n} \quad (26)$$

$$i_D(t)=i_{Lr}(t)=I_L-\frac{V_i+(n-1)V_o}{nL_r}(t-t_3) \quad (27)$$

Stage 5 (t_4–t_5): The leakage inductor current i_{Lr} and diode current i_D decay to zero at t_4. Owing to the leakage inductor L_r, the reverse-recovery problem of the main diode is greatly alleviated. Then, L_r resonates with C_{eq} as shown in (28).

$$\begin{cases} L_r\dfrac{di_{Lr}(t)}{dt}=\dfrac{(n-1)(V_i-V_o)}{n}-v_{ds}(t) \\ C_{eq}\dfrac{dv_{ds}(t)}{dt}=i_{Lr}(t) \end{cases} \quad (28)$$

Stage 6 (t_5–t_6): The voltage v_{ds} decreases to zero at t_5, and the current i_{Lr} flows through the body diode of S_1; hence, S_1 is ZVS turned on. The leakage inductor voltage v_{Lr}, shown in (29), must be larger than zero to increase the leakage inductor current i_{Lr} to the magnetizing current I_L. Therefore, the turns ratio n should be larger than 1. And from (14), the auxiliary current i_a decreases.

$$v_{Lr}=\frac{(n-1)(V_i-V_o)}{n} \quad (29)$$

$$n>1 \quad (30)$$

$$i_S(t)=i_{Lr}(t)=i_{Lr}(t_5)+\frac{(n-1)(V_i-V_o)}{nL_r}(t-t_5) \quad (31)$$

Stage 7 (t_6–t_7): At t_6, i_{Lr} rises to zero. This stage is similar with the stage 6 except that the leakage inductor current i_{Lr} is positive. The switching period ends at t_7 when the auxiliary current i_a drops to zero.

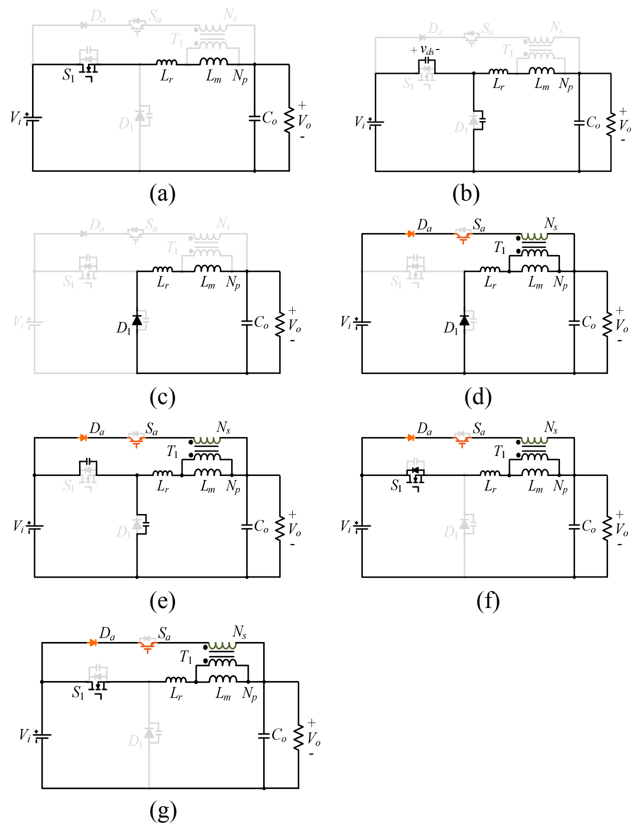

Fig. 5. Equivalent circuits of the magnetic coupling ZVS buck converter: (a) stage 1, (b) stage 2, (c) stage 3, (d) stage 4, (e) stage 5, (f) stage 6, and (g) stage 7.

IV. ANALYSIS AND COMPARISON

A. Voltage Gain

Owing to the flux balance, the average voltage across the leakage inductor L_r and magnetizing inductor L_m in a switching period is zero. Therefore, the output voltage V_o is equal to the average diode voltage V_D. From Fig. 4(b), the voltage gain of the proposed converter is derived in (32), which is similar with that of the conventional buck converter.

$$M=\frac{V_o}{V_i}=\frac{V_D}{V_i}\approx D \quad (32)$$

B. Average Magnetizing Current IL

From the operation principle in section III, the leakage inductor current i_{Lr} in different stage is summarized in (33). Then the relationship between the average leakage inductor current I_{Lr} and magnetizing current I_L can be derived. Combing with (34) derived from (14) and (15), I_L can be calculated in terms of average output current I_o. The relationship between I_L and I_o with L_r=6 μH and n=1.5 as a function of voltage gain M is illustrated in

Fig. 6. The average magnetizing current I_L is a little larger than the average output current I_o, but the difference is small, particularly at a low voltage gain M.

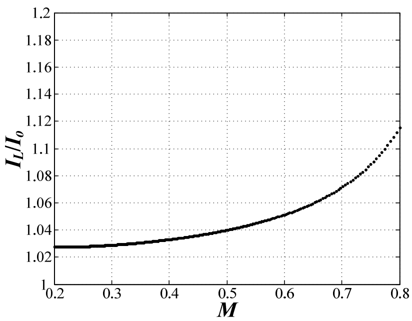

Fig. 6. Relationship between I_L and I_o as a function of voltage gain M.

$$i_{Lr}(t)=\begin{cases} I_L & (t_0\sim t_3)\\ I_L-\dfrac{V_i+(n-1)V_o}{nL_r}(t-t_3) & (t_3\sim t_4)\\ -\omega C_{eq}\dfrac{V_i+(n-1)V_o}{n}\sin\omega(t-t_4) & (t_4\sim t_5)\\ i_{Lr}(t_5)+\dfrac{(n-1)(V_i-V_o)}{nL_r}(t-t_5) & (t_5\sim t_7)\end{cases} \quad (33)$$

$$(n-1)I_{Lr}+I_L=nI_o \quad (34)$$

C. Voltage Stress

The turn-off voltage of the main switch S_1 and diode D_1 is clamped by the input voltage V_i, which is the same as the conventional buck converter. In the stage 1, the auxiliary diode D_a is reverse biased and the turn-off voltage is given in (36) with the neglect of the leakage inductance L_r, which is much smaller than the magnetizing inductance L_m. Likewise, the auxiliary switch S_a is turned off in the stage 3, and the voltage stress is derived in (37).

$$V_{S1}=V_{D1}=V_i \quad (35)$$

$$V_{Da}=nv_{Lm}-(V_i-V_o)=(\frac{nL_m}{L_r+L_m}-1)(V_i-V_o) \approx (n-1)(V_i-V_o) \quad (36)$$

$$V_{Sa}=V_i-V_o-nv_{Lm}=V_i-V_o-n\frac{L_m}{L_m+L_r}(-V_o) \approx V_i+(n-1)V_o \quad (37)$$

D. Current Stress

According to Fig. 4(b), in the intervals [t_5, t_7] and [t_0, t_1], the main switch S_1 conducts and the current i_S is equal to the leakage inductor current i_{Lr}. Therefore, the RMS current of the main switch is derived in (38). In the interval [t_2, t_4], the leakage inductor current i_{Lr} flows through the main diode D_1 and hence the average current I_{D1} is given in (39). Similarly, the RMS current of the auxiliary switch $I_{a,RMS}$ and the average current of the auxiliary diode $I_{a,ave}$ can be obtained, as illustrated in (40) and (41).

$$I_{S_1,RMS}=\frac{1}{T_s}\sqrt{\int_{t_5}^{t_7} i_{Lr}^2(t)dt+\int_{t_0}^{t_1} i_{Lr}^2(t)dt} \quad (38)$$

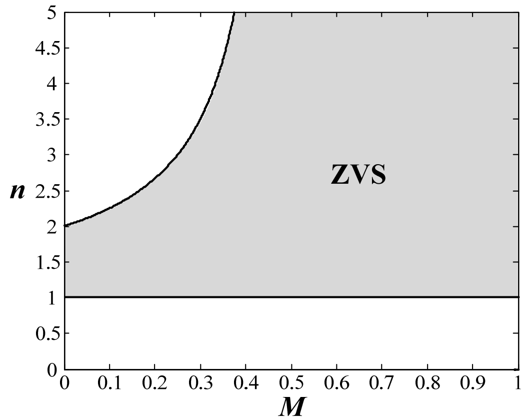

Fig. 7. Available turns ratio n to achieve ZVS as a function of M.

$$I_{D1}=\frac{1}{T_s}\int_{t_3}^{t_4} i_{Lr}(t)dt \quad (39)$$

$$I_{a,RMS}=\frac{1}{T_s}\sqrt{\int_{t_3}^{t_7}\frac{1}{n^2}(I_L-i_{Lr}(t))^2dt} \quad (40)$$

$$I_{a,ave}=\frac{1}{T_s}\int_{t_3}^{t_7}\frac{1}{n}(I_L-i_{Lr}(t))dt \quad (41)$$

E. Soft-switching Analysis

For the proposed buck converter, in order to achieve ZVS for the main switch S_1, (42) must be satisfied from (12) and Table I. Combining with n>1 in (30), the available value of turns ratio n at different voltage gain M is depicted in Fig. 7. With $1<n\le 2$, the main switch can theoretically realize ZVS over the whole input voltage range.

$$n(V_i-2V_o)<2(V_i-V_o) \quad (42)$$

In practical, the maximum current $I_{L,max}$ is restricted in (11) and (13) to realize ZVS operation over the whole load range with a fixed phase angle φ for the Class-B ZVT buck converter in Fig. 1(a) and the proposed converter, respectively. Fig. 8 depicts the relationship between $I_{L,max}$ and the voltage gain M with different turns ratios n. The available ZVS load range for the ZVT buck converter in Fig. 1(a) is narrow and deteriorated with the increase of auxiliary inductance L_a, which is significantly improved in the proposed ZVS buck converter. Moreover, with the decrease of turns ratio n, the available load range is enlarged. Therefore, the proposed buck converter can achieve ZVS operation for the main switch over both wide input voltage range and large load variation.

The decreasing ratio of the diode current i_D and auxiliary current i_a is limited by the leakage inductor L_r, as illustrated in Fig. 4(b). Therefore, the reverse-recovery problem of diodes D_1 and D_a is greatly alleviated. Moreover, the auxiliary switch S_a is ZCS turned off in the stage 1 since the auxiliary current i_a already decays to zero at t_0.

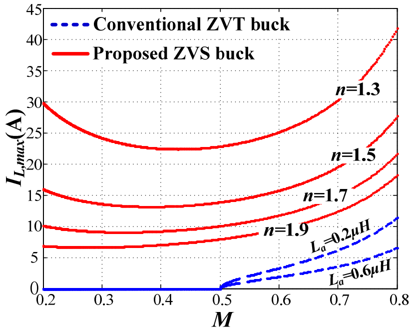

Fig. 8. Maximum magnetizing current $I_{L,max}$ to achieve ZVS over whole load range with a fixed φ for different converters.

F. Comparison

The comparison results between the proposed and other ZVS buck converters are shown in Table III. The QRC buck converter in [4] is considerably simple and does not require an auxiliary switch, but the voltage stress of the main switch is excessively high. In [6], the voltage stress was reduced in the active-clamping buck converter, but it remained higher than that of the input voltage V_i. Moreover, the circulating current is large; thus, conduction losses are deteriorated. The ZVT buck converter in [17] can effectively reduce conduction losses because the auxiliary circuit is removed from the main circuit and only activated in a short interval. However, ZVS operation is lost in the application with V_o<0.5V_i. Nevertheless, all aforementioned converters need an auxiliary inductor. In the proposed buck converter, the ZVS operation can be achieved over wide input voltage range and load variation with the benefits of low voltage stress on the main switch, small circulating current and reduced magnetic component.

V. Experimental Validation

In order to verify the effectiveness of the proposed topology, a 500 W prototype circuit of the magnetic coupling ZVS buck converter with topology parameters in Table II is built. The soft-switching characteristics of the converter are assessed at different input voltages 200 and 300 V under 10% and 100% load variations with open-loop experimental results, respectively.

TABLE II
Parameter Specification

Parameter	Symbol	Value	Units
Input voltage	V_i	200–300	V
Output voltage	V_o	120	V
Rated output power	$P_{o,\max}$	500	W
Switching frequency	f_s	100	kHz
Turns ratio	1:n	1:1.5	
Magnetizing inductance	L_m	1000	μH
Leakage inductance	L_r	5.8	μH
Main switch	S_1	IPW60R190E	
Main diode	D_1	MUR860	
Auxiliary switch	S_a	IKA15N65H5	
Auxiliary diode	D_a	8ETH03	

The steady-state experiment waveforms at 100% load with input voltages V_i=200 V and V_i=300 V are shown in Fig. 9, Fig. 10 and Fig. 11, which are in well coincidence with the theoretical analysis. In Fig. 9, the leakage inductor current i_{Lr} decreases after the turn-on of auxiliary switch S_a to achieve ZVS turn-on for the main switch S_1 , and then rapidly reset to the magnetizing current I_L. The auxiliary circuit is only activated in a short interval, and thus the additional conduction loss is reduced. It is noteworthy that the auxiliary current i_a increases slightly and that the leakage inductor current i_{Lr} decreases after the turn-off of the main switch S_1 due to the influence of the RCD, which is in parallel with the auxiliary switch S_a. From Fig. 10, ZVS is achieved for the main switch S_1 at both input voltages. Moreover, the reverse-recovery problem of the main diode D_1 is greatly alleviated. In addition, as shown in Fig. 11, the ZCS of the auxiliary switch S_a is obtained, which is also independent of the input voltage. Therefore, the proposed ZVS buck converter achieves desirable soft-switching characteristics over a wide input voltage range.

TABLE III
Comparison of the Proposed ZVS Buck Converter and Other ZVS Buck Converters

	Voltage Stress		ZVS Limitation	Magnetic Component	Auxiliary Switch	Circulating Current
	Main Switch	Main Diode				
QRC [4]	$V_i + I_o\sqrt{L_r / C_{ds}}$	V_i	No	2	---	Large
Active-clamping [6]	$V_i/(1\text{-}D)$	V_i	No	2	ZVS	Large
ZVT [17]	V_i	V_i	V_o >0.5V_i	2	ZCS	Small
Proposed	V_i	V_i	No	1	ZCS	Small

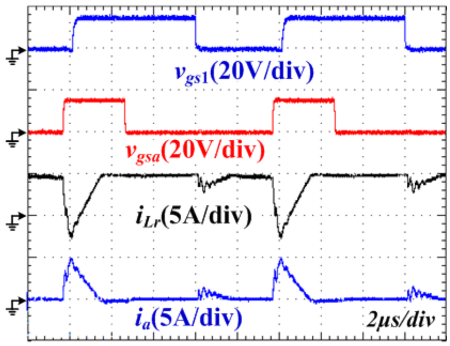

(a)

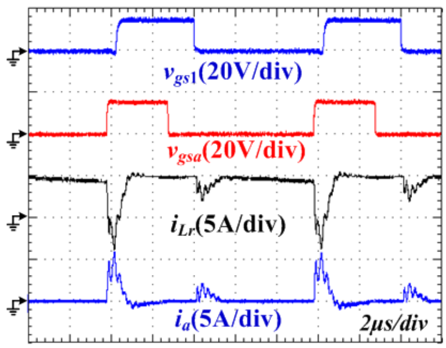

(b)

Fig. 9. Experiment waveforms of drive signals v_{gs1}–v_{gsa}, leakage inductor current i_{Lr}, and auxiliary current i_a, at 100% load with different input voltages: (a) V_i=200 V and (b) V_i=300 V.

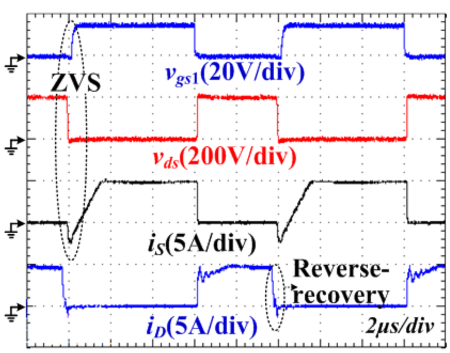

(a)

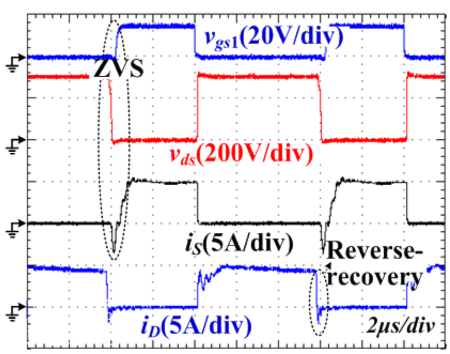

(b)

Fig. 10. Experiment waveforms of drive signals v_{gs1}, drain-to-source voltage v_{ds}, current i_S, and diode current i_D at 100% load with different input voltages: (a) V_i=200 V and (b) V_i=300 V.

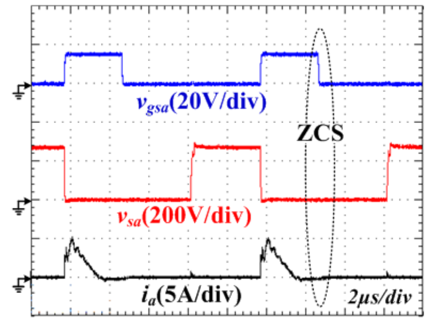

(a)

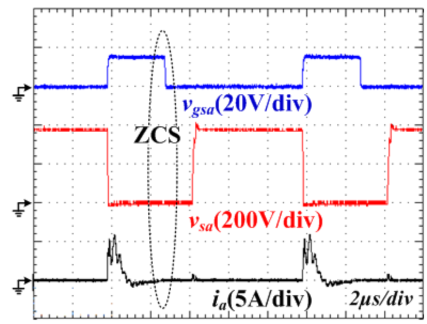

(b)

Fig. 11. Experiment waveforms of drive signals v_{gsa}, drain-to-source voltage v_{sa}, and current i_a at 100% load with different input voltages: (a) V_i=200 V and (b) V_i=300 V.

The experiment waveforms of the main switch S_1 and auxiliary switch S_a at 10% load condition with input voltages V_i=200 V and V_i=300 V are illustrated in Fig. 12 and Fig. 13, respectively. ZVS and ZCS operation are also achieved. Note that the resonance caused by the non-ideality of semiconductor devices and parasitic inductances during the turn-on process of S_1 has slight influence on the ZVS operation, e.g. the drain-to-source voltage v_{ds} increases slightly as shown in Fig. 12(b). Nevertheless, v_{ds} finally decays to zero before the turn-on of S_1. Therefore, improved soft-switching characteristics of the proposed converter remain regardless of the load variation.

The measured efficiency of the proposed magnetic coupling buck converter at V_i=200 V and V_i =300 V is shown in Fig. 14(a), which achieves a maximum value of 97.2%. Thanks to the desirable soft-switching characteristic and the small auxiliary circuit conduction loss, the efficiency of the proposed converter is much improved over whole load range at both input voltages, in comparison with the conventional buck converter, as illustrated in Fig. 14(b)-(c). Compared with the ZVT buck converter in Fig. 1(a), the proposed converter achieves a slightly lower efficiency under heavy load with input voltage V_i=200 V in Fig. 14(b). Nevertheless, the efficiency of the ZVT converter under light load is harshly decreased, resulting from the loss of ZVS with a fixed phase angle φ . Moreover, at V_i=300 V in Fig. 14(c), ZVS operation is still obtained in the proposed ZVS buck converter but lost in the ZVT buck converter. Therefore, the

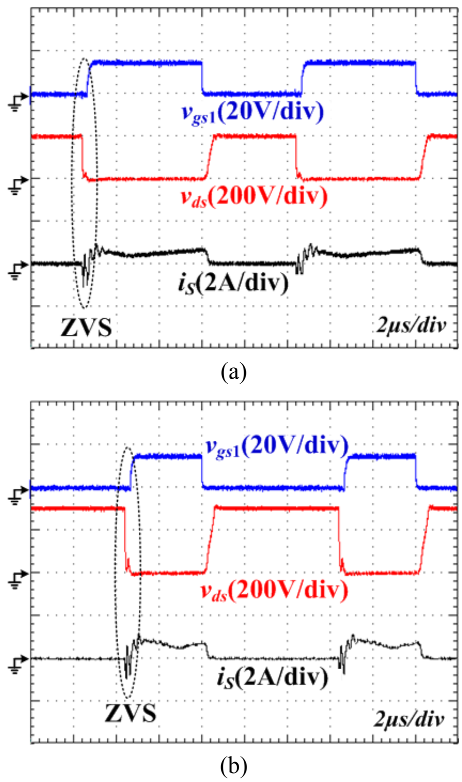

Fig. 12. Experiment waveforms of the drive signal v_{gs1}, drain-to-source voltage v_{ds}, and current i_S at 10% load with different input voltages: (a) V_i=200 V and (b) V_i=300 V.

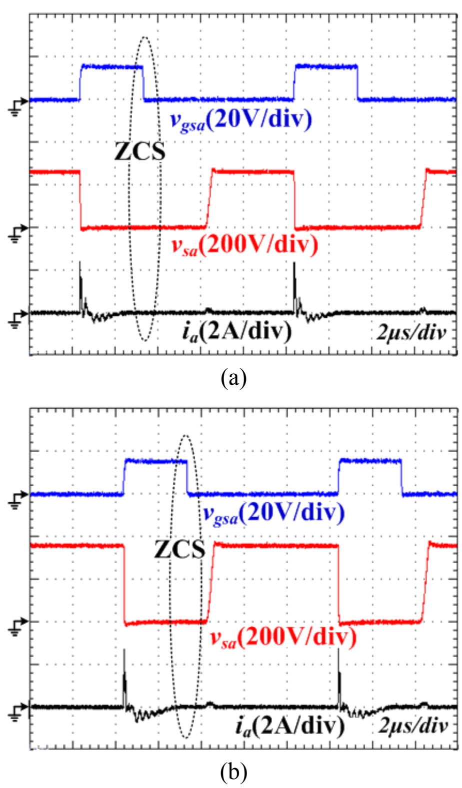

Fig. 13. Experiment waveforms of the drive signal v_{gsa}, drain-to-source voltage v_{sa}, and current i_a at 10% load with different input voltages: (a) V_i=200 V and (b) V_i=300 V.

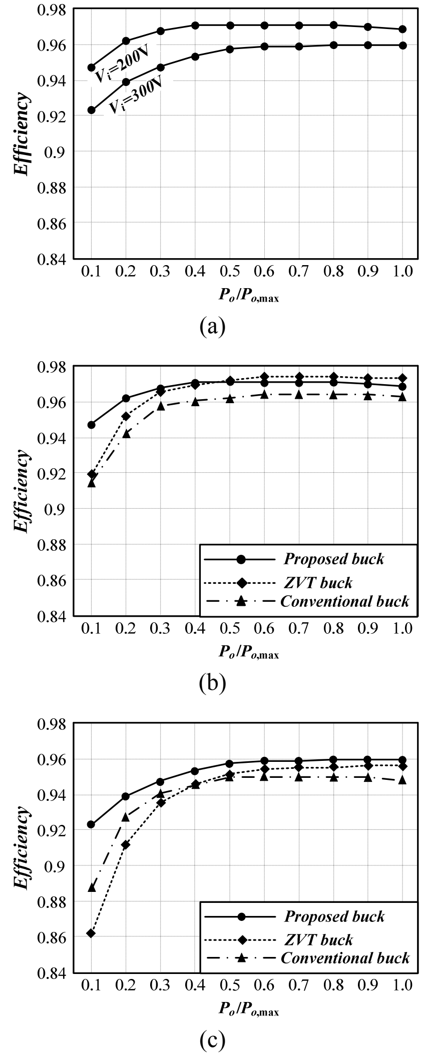

Fig. 14. Measured efficiency: (a) proposed converter at V_i=200 V and V_i =300 V, (b) comparison at V_i =200 V, and (c) comparison at V_i =300 V.

Fig. 15. Photograph of the prototype circuit.

efficiency of the proposed converter is higher than that of the ZVT converter at V_i=300 V. A photograph of the prototype circuit is shown in Fig. 15.

VI. Conclusions

A family of magnetic coupling ZVS buck, boost and buck-boost converters is proposed. Thanks to the additional auxiliary voltage source provided by the coupled inductor, ZVS operation is achieved for the main switch over wide input voltage range and load variation with a reduced magnetic component. Besides, the auxiliary circuit obtains the advantages of ZCS operation and small circulating current. The proposed ZVS buck converter is taken as an example to clearly introduce the operation principle and analysis. Experiment waveforms and measured efficiency based on a 500 W prototype circuit at input voltages of 200 V and 300 V under 10% and 100% load conditions are given to validate converter performance.

ACKNOWLEDGMENT

This work was sponsored by the National Natural Science Foundation of China (51377144).

REFERENCES

[1] O. Ellabban, J. V. Mierlo, and P. Lataire, "A DSP-based dual loop digital controller design and implementation of a high power boost converter for hybrid electric vehicles applications," *Journal of Power Electronics*, Vol. 11, No. 2, pp.113-119, Mar. 2011.

[2] Y. Zhang, J. Liu, X. Ma, and J. Feng, "Comparison of conventional DC-DC converter and a family of diode-assisted DC-DC converter in renewable energy applications," *Journal of Power Electronics*, Vol. 14, No. 2, pp. 203-216, Mar. 2014.

[3] E. Jayashree and G. Uma, "Design and implementation of zero-voltage-switching quasi-resonant positive-output Luo converter using analog resonant controller UC3861," *IET Power Electronics*, Vol. 4, No. 1, pp. 81-88, Jan. 2011.

[4] Y. C. Chuang and Y. L. Ke, "A novel high-efficiency battery charger with a buck zero-voltage-switching resonant converter," *IEEE Trans. Energy Convers*., Vol. 22, No. 4, pp. 848–854, Dec. 2007.

[5] K. H. Liu and F. C. Y. Lee, "Zero-voltage switching technique in DC/DC converters," *IEEE Trans. Power Electron*., Vol. 5, No. 3, pp. 293-304, Jul. 1990.

[6] C. Nan, R. Ayyanar, and Y. Xi, "High frequency active-clamp buck converter for low power automotive applications," in *IEEE Energy Conversion Congress and Exposition (ECCE)*, pp. 3780-3785, Sep. 2014.

[7] S. S. Lee, S. W. Choi, and G. W. Moon, "High efficiency active clamp forward converter with synchronous switch controlled ZVS operation," *Journal of Power Electronics*, Vol. 6, No. 2, pp.131-138, Mar. 2006.

[8] Y. Hu, W. Xiao, W. Li, and X. He, "Three-phase interleaved high-step-up converter with coupled-inductor-based voltage quadrupler," *IET Power Electronics*, Vol. 7, No. 7, pp. 1841-1849, Jul. 2014.

[9] B. R. Lin and C. L. Huang, "Zero voltage switching active clamp buck-boost stage Cuk converter," *IET Electric Power Applications*, Vol. 1, No. 2, pp. 173-182, Mar. 2007.

[10] C. M. C. Duarte and I. Barbi, "An improved family of ZVS-PWM active-clamping DC-to-DC converters," *IEEE Trans. Power Electron*., Vol. 17, No. 1, pp. 1-7, Jan. 2002.

[11] M. L. Martins, J. L. Russi, and H. L. Hey, "Zero-voltage transition PWM converters: a classification methodology," *IEE Proceedings - Electric Power Applications*, Vol. 152, No. 2, pp. 323-334, Mar. 2005.

[12] G. Hua, C. S. Leu, Y. Jiang, and F. C. Y. Lee, "Novel zero-voltage-transition PWM converters," *IEEE Trans. Power Electron.*, Vol. 9, No. 2, pp. 213-219, Mar. 1994.

[13] I. Lee, J. Kim, T. Lee, Y. Jung, and C. Won, "A new bidirectional DC-DC converter with ZVT switching," in *IEEE Vehicle Power and Propulsion Conference*, pp. 684-689, Oct. 2012.

[14] J. Yang and H. Do, "High-efficiency bidirectional DC–DC converter with low circulating current and ZVS characteristic throughout a full range of loads," *IEEE Trans. Ind. Electron.*, Vol. 61, No. 7, pp. 3248-3256, Jul. 2014.

[15] I. D. Kim, S. H. Choi, E. C. Nho, and J. W. Ahn, "A simple ZVT PWM single-phase rectifier with reduced conduction loss and unity power factor," *Journal of Power Electronics*, Vol. 7, No. 1, pp.55-63, Jan. 2007.

[16] J. L. Russi, M. L. S. Martins, H. A. Graundling, H. Pinheiro, J. R. Pinheiro, and H. L. Hey, "A unified design criterion for ZVT DC-DC PWM converters with constant auxiliary voltage source," *IEEE Trans. Ind. Electron*., Vol. 52, No. 5, pp. 1261-1270, Oct. 2005.

[17] J. E. Baggio, L. Schuch, H. L. Hey, H. A. Grundling, H. Pinheiro, and J. R. Pinheiro, "Quasi-ZVS active auxiliary commutation circuit for two switches forward converter," in *IEEE 32nd Annual Power Electronics Specialists Conference (PESC)*, Vol. 1, pp. 398-403, Jun. 2001.

[18] N. P. Filho, V. J. Farias, L. Carlos, and L. C. de Freitas, "A novel family of DC-DC PWM converters using the self-resonance principle," in *IEEE 25th Annual Power Electronics Specialists Conference (PESC)*, Vol. 2, pp. 1385-1391, Jun. 1994.

[19] M. L. S. Martins, J. L. Russi, and H. L. Hey, "Novel design methodology and comparative analysis for ZVT PWM converters with resonant auxiliary circuit," *IEEE Trans. Ind. Appl.*, Vol. 42, No. 3, pp. 779-796, May/Jun. 2006.

[20] K. Ogura, S. Chandhaket, T. Ahmed, and M. Nakaoka, "ZVS-PWM Boost chopper-fed DC-DC converter with load-side auxiliary edge resonant snubber and its performance evaluations," *Journal of Power Electronics*, Vol. 4, No. 1, pp. 46-55, Jan. 2004.

[21] H. Mao, O. A. Rahman, and I. Batarseh, "Zero-voltage-switching DC–DC converters with synchronous rectifiers," *IEEE Trans. Power Electron*., Vol. 23, No. 1, pp. 369-378, Jan. 2008.

[22] J. L. Russi, M. L. D. S. Martins, L. Schuch, J. R. Pinheiro, and H. L. Hey, "Synthesis methodology for multipole ZVT converters," in *37th IEEE Power Electronics Specialists Conference*, pp. 1-7, Jun. 2006.

[23] H. L. Do, "Zero-voltage-switching boost converter using a coupled inductor," *Journal of Power Electronics*, Vol. 11, No. 1, pp. 16-20, Jan. 2011.

[24] H. L. Do, "Zero-voltage-switching synchronous buck converter with a coupled inductor," *IEEE Trans. Ind. Electron.*, Vol. 58, No. 8, pp. 3440-3447, Aug. 2011.

[25] X. Zhang, L. Jiang, J. Deng, and S. Li, "Analysis and design of a new soft-switching boost converter with a coupled inductor," *IEEE Trans. Power Electron*., Vol. 29, No. 8, pp. 4270-4277, Aug. 2014.

[26] G. Chen, Y. Deng, X. He, Y. Wang, and J. Zhang, "Zero-voltage-switching buck converter with low-voltage stress using coupled inductor," *IET Power Electronics,* Vol. 9, No. 4, pp. 719-727, Mar. 2016.

[27] A. Rahimi and M. R. Mohammadi, "Zero-voltage-transition synchronous DC–DC converters with coupled inductors," *Journal of Power Electronics*, Vol. 16, No. 1, pp. 74-83, Jan. 2016.
[28] M. R. Mohammadi and H. Farzanehfard, "New family of zero-voltage-transition PWM bidirectional converters with coupled inductors," *IEEE Trans. Ind. Electron*., Vol. 59, No. 2, pp. 912-919, Feb. 2012.

Guipeng Chen received his B.E.E. degree from the Department of Electrical Engineering, Zhejiang University, Hangzhou, China, in 2011. He is currently working toward his Ph. D degree at the College of Electrical Engineering, Zhejiang University, Hangzhou, China. His current research interests include soft-switching DC–DC converters, bidirectional DC–DC converters, and multi-port DC–DC converters.

Jie Dong received her B.E.E degree from the School of Electronic Information and Electrical Engineering, Shanghai Jiaotong University, Shanghai, China, in 2014. She is currently working toward her MA. Sce degree at the College of Electrical Engineering, Zhejiang University, Hangzhou, China.

Yan Deng received his B.E.E. degree from the Department of Electrical Engineering, Zhejiang University, Hangzhou, China, in 1994, and his Ph.D. degree in Power Electronics and Electric Drives from the College of Electrical Engineering, Zhejiang University, in 2000. Since 2000, he has been a faculty member at Zhejiang University, where he teaches and conducts research on power electronics. He is currently an Associate Professor. His research interests are topologies and control for switch-mode power conversion.

Yong Tao received his B. Sc. Degree in Electrical Engineering from Nanjing University of Science and Technology, Nanjing, China, in 2011. He is currently working toward his Ph.D. degree at the College of Electrical Engineering, Zhejiang University, Hangzhou, China. His research interests include microgrid control, distributed generation, and energy management.

Xiangning He received his B.Sc. and M.Sc. degrees from Nanjing University of Aeronautical and Astronautical, Nanjing, China, in 1982 and 1985, respectively, and his Ph.D. degree from Zhejiang University, Hangzhou, China, in 1989. From 1989 to 1991, he was a Lecturer at Zhejiang University. In 1991, he obtained a fellowship from the Royal Society of the U.K. and conducted research at Heriot-Watt University, Edinburgh, U.K., as a Post-Doctoral Research Fellow for two years. In 1994, he joined Zhejiang University as an Associate Professor. Since 1996, he has been a Full Professor at Zhejiang University. He is currently the Vice Dean of the College of Electrical Engineering, Zhejiang University. His research interests are power electronics and their industrial applications. He has published more than 280 papers and holds 22 patents.

Yousheng Wang was born in 1928. He received his B.S. degree from the Department of Electrical Engineering, Zhejiang University, Hangzhou, China.

In 1950, he joined the Department of Electrical Engineering of Zhejiang University as a faculty member. He became a Professor in 1978. His research interests include power electronics and high-frequency induction heating. Mr. Wang received several national awards for his outstanding work in large electric generators and static induction heating equipment. He is a member of the China Academy of Engineering.